ADVANCED FUNCTIONAL MATERIALS
www.afm-journal.de

Breathable and Flexible Polymer Membranes with Mechanoresponsive Electric Resistance

Qiang Gao, Bernd A. F. Kopera, Jian Zhu, Xiaojian Liao, Chao Gao, Markus Retsch, Seema Agarwal, and Andreas Greiner**

Flexible low-resistance membranes play an important role in soft electronics as sensors for robotics, body movement monitoring, nanogenerators to collect kinetic energy from body movements, and flexible batteries. Despite great efforts, low-resistance, mechanically stable large-dimensional membranes that tolerate very high deformability without sacrificing resistance produce low joule heating and allow passage of gases for human comfort are still being sought. Here, one of the solutions is provided by sandwiching a network of silver nanowires (AgNWs) between two highly porous electrospun thermoplastic polyurethane (TPU) membranes. The membranes are mechanically robust (both for bending and stretching) with a strong interface and large strain before breakage (more than 700%). The sheet resistance is as low as <0.1 (±0.01) Ω sq^{-1}, and changed to only 1.6 (±0.43) Ω sq^{-1} upon stretching to 100% strain. The combination of polymer elasticity and the AgNW network structure provides a reversible change in resistance beyond 100% strain. A detailed thermographic analysis is employed to in situ image and characterize the AgNW network morphology during various stretched conditions. It is believed that this flexible, sandwich-like, electrically conductive membrane is a good candidate for smart wearable devices and soft robots.

1. Introduction

Traditional electronics are typically composed of intrinsically heavy and rigid materials, like silicon, metals, and glass, that have extremely limited flexibility, stretchability, bendability, twistability, and impact resistance. There is great need for flexible and deformable circuits and electrodes with low electric resistance that maintain performance even at strained state because of the current rapid development of lightweight, wearable, and flexible electronic devices.[1] Efforts to construct flexible circuits and electrodes with low resistance focused on elastomeric electrically conductive materials. Examples include electrically conductive sponges,[2] hydrogels,[3] nonwovens,[4] films,[5] and fibers.[6] These materials are promising for energy production and storage,[7] actuators,[8] sensors,[9] electronic skin,[10] and soft robotics.[11] However, obtaining flexible conductors with both high strain properties and low resistance is a challenge for design and production of flexible electronic devices.[12] Further, porosity is an important requirement in case electronic devices are meant for contact with skin. Air permeability is very important for the comfort of wearable devices. Achieving a combination of flexibility, elasticity, high conductivity, in porous membranes with good mechanical integrity is a continued search.

Presently, typical flexible electrodes are composed of an elastic substrate as the elastomer to support bending, stretching, and twisting. The most commonly used materials

Q. Gao, J. Zhu, X. Liao, Prof. S. Agarwal, Prof. A. Greiner
Macromolecular Chemistry and Bavarian Polymer Institute
University of Bayreuth
Universitätsstrasse 30, 95440 Bayreuth, Germany
E-mail: greiner@uni-bayreuth.de

B. A. F. Kopera, Prof. M. Retsch
Department of Chemistry
Physical Chemistry I and Bavarian Polymer Institute
University of Bayreuth
Universitätsstrasse 30, 95440 Bayreuth, Germany
E-mail: markus.retsch@uni-bayreuth.de

The ORCID identification number(s) for the author(s) of this article can be found under https://doi.org/10.1002/adfm.201907555.

DOI: 10.1002/adfm.201907555

Prof. C. Gao
MOE Key Laboratory of Macromolecular Synthesis and Functionalization
Department of Polymer Science and Engineering
Institute of Applied Mechanics
State Key Laboratory of Fluid Power and Mechatronic Systems
Zhejiang University
Hangzhou 310027, P. R. China

Prof. C. Gao
Hangzhou Gaoxi Technology Co., Ltd.
Hangzhou 310027, P. R. China

are: polydimethylsiloxane (PDMS),[13] thermoplastic polyurethane (TPU),[14] electrically conductive polymers,[15] carbon materials,[16] metal nanoparticles,[17] and metal nanowires.[18] Technically, low-resistance electrodes provide the advantages of less energy loss and joule heating. Silver is an excellent material for electrodes and is often used for flexible electrodes with low resistance.[19] In our previous work, we prepared electrospun polymer membranes with a metal-like conductivity of 7.5×10^5 S m^{-1} using a very low content of silver nanowires (AgNWs: 3.35 vol%) as an additive.[4] However, this kind of electrically conductive membrane is bendable but not sufficiently stretchable.

To prepare flexible membranes, printing fabrication techniques have been developed by transferring electrically conductive materials from a working substrate to another target substrate, such as PDMS, TPU, and polyethylene terephthalate (PET).[20] Additionally, printing fabrication techniques provide a simple and versatile way to design and print patterns on substrate materials using computer control.[14,21] In addition, microfluidic processing,[22] microchannel wetting patterning,[23] direct laser patterning,[24] shadow mask patterning,[25] and photolithographic[26] methods have also been developed to fabricate flexible conductors. Other methods, such as filling of a AgNW network prepared by spray drying of a AgNW dispersion with PDMS was also used for making stretchable, conductive electrodes.[13b] Nevertheless, the stretchable conductors prepared with these methods are all airtight due to their nonporous elastic substrate.

Alternatively, electrospinning is a promising technique for fabricating porous substrates with high conductivity, flexibility, and air permeability. The good electrospinnability of many different polymer types also provides the advantage of tuning the membrane mechanical characteristics. For example, electrospun polyamide nanofiber nonwovens embedded with AgNW networks showed 50% stretchability and a sheet resistance of 8.2 Ω sq^{-1}.[27] Electrospun polyurethane nonwoven porous substrate coated with AgNW provided highly stretchable membrane (more than 300%) with high conductivity.[28]

Here, we present a flexible and breathable polymer membrane with bending/stretching stability and very low electrical resistance as a new electrode material. Also, we provide important fundamental studies regarding analysis on island formation, evolution of anisotropy and hot-spots, and thermal transport in such structures. Our study shows 1) a simple preparation method for making such membranes which is applicable to large-dimension samples. We use a network of AgNWs as conductive layer sandwiched between two porous TPU fibrous nonwovens made by electrospinning. We improved the interface stability with polycaprolactone (PCL) hot glue in the form of short fibers dispersed in between the AgNW network. 2) Our membranes show a sheet resistance as low as <0.1 Ω sq^{-1}. The resistance does not significantly increase upon deformation (twisting, bending and stretching to approximately 100% strain). 3) We also show a reversible change in the resistance upon stretching or bending with more than 100% strain for several cycles. The AgNW networks reversibly breaks and reforms during stretching and releasing, respectively. 4) Our membranes are breathable. This allows the exchange of gases, which is important for human comfort. 5) Our membranes are thermal insulators comparable to porous polymers, despite their electrical conductivity. We think that our membranes are a promising material for electrodes in smart textiles and other wearable devices.

2. Results and Discussion

The concept for the preparation of flexible and breathable electrically conductive membranes is illustrated in **Figure 1**. First, we prepared TPU nanofiber nonwovens via

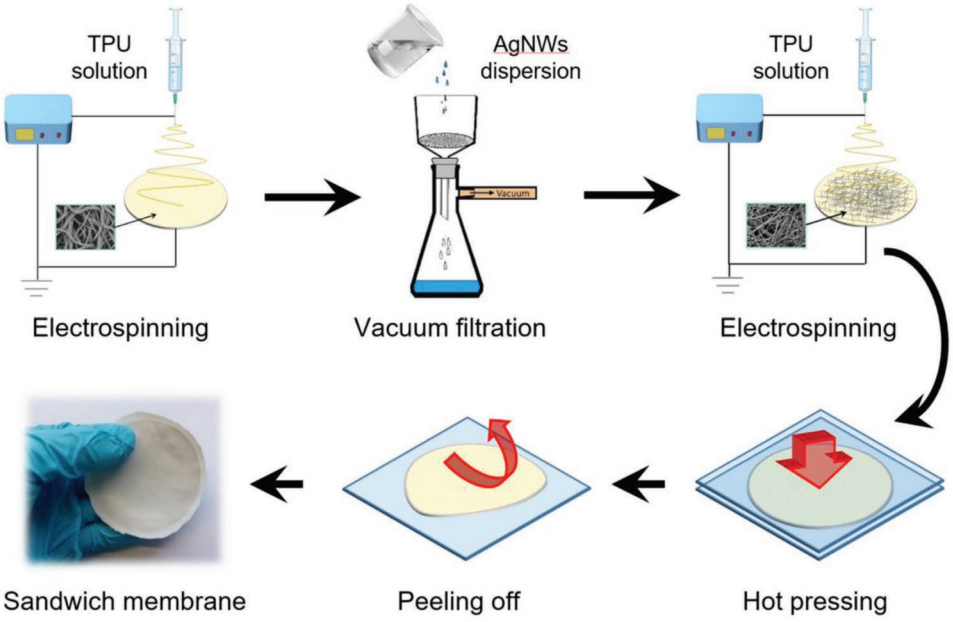

Figure 1. Schematic of preparing the TPU-AgNW/PCL-TPU membrane by sandwiching a network of AgNWs between TPU layers.

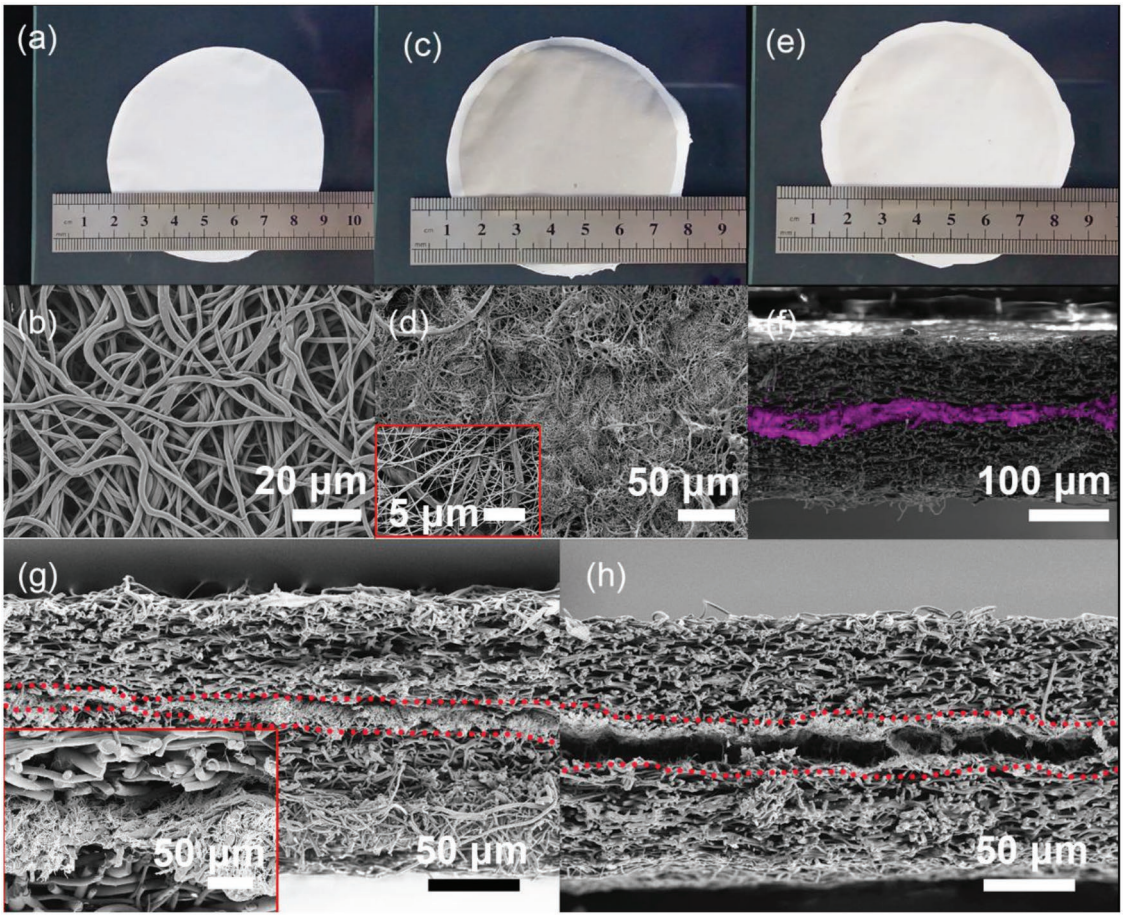

Figure 2. Photograph a) and SEM image b) of the electrospun TPU nonwoven. Photograph c) and SEM image d) of the electrospun TPU nonwoven layered with AgNWs and PCL after heating. Photograph of as-prepared sandwich membrane of TPU-AgNW/PCL-TPU e). Cross-section of EDX overlapped SEM image of as-prepared sandwich membrane of TPU-AgNW/PCL-TPU with PCL short fibers f). Cross-section of TPU-AgNW/PCL-TPU g) and TPU-AgNW -TPU h).

electrospinning. We then used the porous TPU membranes as a filter for the filtration of AgNWs (17 mg mL^{-1}, 126 ± 10 nm in diameter and 18 ± 4 μm in length, Figure S1, Supporting Information) mixed with a PCL short-fiber dispersion (1 mg mL^{-1}, average aspect ratio ≈1000, Figure S2, Supporting Information). The TPU nonwovens consist of randomly oriented fibers (the 2D order parameter is around 0.1) with an average diameter of 1.6 ± 0.5 μm (**Figure 2**a,b). After filtration, the AgNWs and short PCL fibers generated a double network-type structure due to percolation (Figure 2c,d). Afterward, we covered the AgNW/PCL layer with another layer of TPU nonwoven by electrospinning. Finally, we hot pressed the three-layer stack at 75 °C for 30 min to melt the PCL and increase the adhesion of the layers (Figure 2e). The resulting three-layer membranes are designated as TPU-AgNW/PCL-TPU. We checked the presence of an AgNW layer sandwiched between the two TPU layers with PCL short fibers by EDX (Figure 2f). The cross-sectional SEM images of TPU-AgNW/PCL-TPU and TPU-AgNW-TPU (without the use of PCL short fibers for comparison) are shown in Figure 2g,h, respectively. The PCL short-fiber dispersion acts as a glue between the AgNW network and the TPU. The importance of providing a good adhesion between the fiber support and the conducting nanowires was also investigated by Jiang et. al.[28] Omitting the PCL left us with a loose interface between the layers. Figure S3, Supporting Information, shows the morphology of the middle layer composed only of PCL short fibers after hot pressing at 75 °C for 30 min. Patches of molten fibers can be observed.

The pore size distribution (Figure S4, Supporting Information) of the sandwich membrane without AgNWs is mainly distributed at 2.8 μm with 80% porosity. Upon formation of the AgNW network layer, the average pore size was 1.5–0.9 μm. Additionally, the thickness of the sandwich membrane increased slightly with increasing volume of the AgNW solution, from 0.18 ± 0.4 to 0.27 ± 0.02 mm, as shown in Figure S5, Supporting Information.

Different amounts of the AgNW dispersion were used to investigate the influence of the AgNW concentration on the air permeability and electrical properties. The relevant parameters are illustrated in **Table 1**. The sheet resistance was as high as $6.1 \pm 0.3 \times 10^8$ Ω sq^{-1} without an AgNW layer. The sheet resistance decreased to as low as 0.09 Ω sq^{-1} upon increasing the amount of AgNWs because of the formation of a dense network of AgNWs. Even the use of a small amount of AgNWs

Table 1. The relevant parameters of flexible sandwich-like electrically conductive membranes with different contents of AgNWs.

Sample	TPU spinning solution (16 wt%) [mL]	PCL dispersion (1 g L^{-1}) [mL]	AgNW dispersion (17 mg mL^{-1}) [mL]	Density [gm^{-2}]	Content of AgNWs [wt%]	Sheet resistance of the AgNW layer [Ω sq^{-1}]
TPU-PCL-TPU	1	10	0	–	–	$6.1 \pm 0.3 \times 10^8$
TPU-0.1AgNW/ PCL-TPU	1	10	0.1	0.51	0.5 ± 0.6	$2.4 \pm 3.1 \times 10^6$
TPU-0.25AgNW/ PCL-TPU	1	10	0.25	1.28	1.2 ± 0.5	1.14 ± 0.15
TPU-0.5AgNW/ PCL-TPU	1	10	0.5	2.56	2.0 ± 0.6	0.39 ± 0.07
TPU-1.0AgNW/ PCL-TPU	1	10	1.0	5.12	3.5 ± 0.4	0.20 ± 0.02
TPU-1.5AgNW/ PCL-TPU	1	10	1.5	7.68	7.9 ± 1.2	0.16 ± 0.04
TPU-2.0AgNW/ PCL-TPU	1	10	2.0	10.24	8.5 ± 1.7	0.09 ± 0.002

– represents no AgNW in the sample.

(1.2 wt%) significantly decreased the resistance to ≈1 Ω sq^{-1}. Further reduction in the amount of AgNW to ≈0.5 wt% led to a sharp increase in the sheet resistance ($2.4 \pm 3.1 \times 10^6$ Ω sq^{-1}). This indicates that the amount of AgNW required for making a network by percolation is somewhere between 0.5 and 1.2 wt%. In general, the sheet resistance of TPU-AgNW/PCL-TPU remains almost unchanged at 100 °C in air for more than 60h (Figure S6, Supporting Information).

The TPU-AgNW/PCL-TPU membranes also possess good gas permeability (Figure S7, Supporting Information), as demonstrated by the penetration of carbon dioxide (CO_2) gas, visualized by the pink base solution containing phenolphthalein indicator (Video S1, Supporting Information).

The sandwich membranes exhibited stress at break of more than 8 MPa. The TPU without AgNWs had a breaking stress of ≈10 MPa. We observed excellent stretchability for the TPU-AgNW/PCL-TPU membranes. The membranes with different amounts of AgNWs can be stretched to over 700% (**Figure 3**a). The membranes showed 10% and 30% creep after stretching for 100 cycles to 50% and 100% strain, respectively (Figure S8, Supporting Information). We measured the resistance as a function of % strain (Figure 3b). TPU-AgNW/PCL-TPU can tolerate considerable strains with a moderate increase in resistance depending upon the amount of AgNWs. The sample with the highest content of AgNWs (TPU-2.0AgNW/PCL-TPU; 8.5 wt%) changed its resistance by only two orders of magnitude at a strain of ≈150%. In contrast, the sample with the fewest AgNWs (TPU-0.25AgNW/PCL-TPU; 1.2 wt%) showed a comparable increase in resistance already at a strain of only 60%. The network was sparse due to fewer AgNWs in TPU-0.25AgNW/PCL, which led to a higher initial sheet resistance and stronger increase in resistance during stretching.

Figure 3c shows the morphologies of the AgNW layer after 0%, 100%, and 150% stretching and recovering to 0% again for the TPU-2.0AgNW/PCL sample (8.5 wt% AgNWs). When the membrane was stretched up to 100%, hardly any cracks could be observed in the AgNW layer. However, upon further stretching to approximately 150%, large cracks (bright area) occurred, causing a significant increase in resistance. The cracks visualize that the AgNW breaks up in an island-like fashion. The formation of island-like structures is confirmed by EDX measurement (Figure 3d). The separated islands and cracks restricted the flow of electricity and in turn created hot spots (Figure S9, Supporting Information) by joule heating at the bottle necks. Such hotspots can be imaged by infrared thermography when applying a DC current (Figure 3e). The hotspots shift with increasing strain and highlight the dynamic changes within the AgNW network upon stretching (see Video S2, Supporting Information). Depending on the overall resistance of the composite sample and local bottle necks this can lead to substantial Joule heating resulting in a fatal failure of the sandwich structure at high strains. For low power applications and in the light of practical strains for the case of wearable electronics our sandwich structure will operate in a safe window with low Joule heating.

The morphological changes of the AgNW network upon stretching cannot be directly assessed, since they are embedded between two layers of TPU fibers. We, therefore, employ direction dependent lock-in thermography to gain a better insight on the composite morphology. Using a line laser as a heat source, we are able to probe the overall thermal diffusivity in such a composite sample along different orientations relative to the stretching direction. We see in **Figure 4**a–c that the TPU fibers align expectedly parallel to the stretching direction. Image analysis of these laser scanning microscopy images reveal that the fiber orientation is already complete at a strain of ≈100%.

The 2D order parameter (S_{2D}) measures how well the fibers are aligned. The order parameter is given by

$$S_{2D} = \frac{2}{N} \cdot \left[\sum_{i=1}^{N} \left(\cos\left(\alpha_i - \bar{\alpha} \right) \right)^2 \right] - 1 \quad (1)$$

where N is the number of stretched fiber orientations in the SEM image, α_i is the angle between the fiber and the horizontal

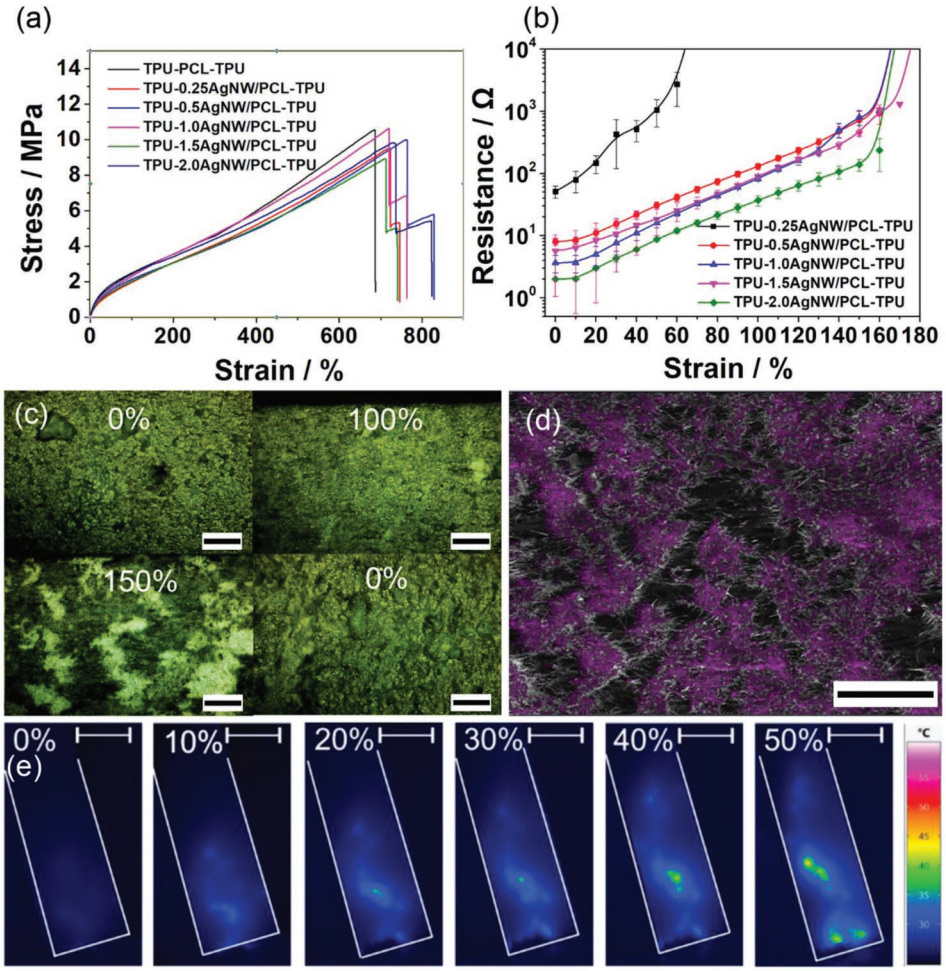

Figure 3. a) Stress–strain curves of sandwich membranes with different amounts of AgNWs. b) Resistance of sandwich membranes with different amounts of AgNWs with different strains. c) Optical images of TPU-2.0AgNW/PCL under different stains. Note the appearance of white spots at 150% strain due to cracks in the AgNW layer. (scale bar: 500 µm) d) EDX-SEM image of TPU-2.0AgNW/PCL at 100% strain. (scale bar: 50 µm) Ag is indicated in purple. e) Thermography images of the TPU sandwich sample upon stretching. White lines indicate the film boundary. A constant current of 2 mA passes through the sample. Note the appearance and shift of hotspots due to local bottlenecks for the electric current created by the cracks in the AgNW layer (scale bars: 3 mm).

axis, and ($\overline{\alpha}$) is the average angle.[29] The 2D order parameter of pure TPU remains constant at a value close to one after 100% strain (Figure 4d). For pure TPU the thermal diffusivity increases along the stretching direction and decreases perpendicular to it (Figure 4e,f). Since TPU is a thermal insulator the absolute thermal diffusivity remains at a low level. The evolution of anisotropy can be explained by the geometric changes, where the fibers start to align, forming an anisotropic fiber network (Figure S10). Heat travels along these oriented fibers faster than perpendicular to it, resulting in a high anisotropy ratio (Figure 4g). The geometric alignment can be accompanied by a molecular orientation of the polymer chains within the fibers, leading to an additional increase in the thermal anisotropy.[30] The thermal diffusivity at 0% strain is higher for the AgNW-TPU sample (TPU-2.0AgNW/PCL-TPU) than for the pure TPU support structure. This can be understood by the additional thermal transport via electronic conduction through the AgNW network. The angular dispersion is rather shallow demonstrating an isotropic temperature spreading in the unstretched and disordered fiber network. Stretching of the fiber network immediately introduces anisotropy to the thermal diffusivity. For AgNW-TPU also some degree of anisotropy evolves (Figure 4h,i), but the thermal diffusivity overall decreases compared to the unstretched state (Figure S11, Supporting Information). This can be understood by a decrease in electronic thermal conductivity in the AgNW layer. The overall thermal diffusivity remains, nevertheless, higher compared to pure TPU. Simultaneously, also for AgNW-TPU samples, we find an evolution of anisotropic heat spreading (Figure 4g). Overall, stretching of the AgNW-TPU sample leads to a smaller amount of anisotropy compared to the pure TPU network structure (Figure 4g). This corroborates our previous findings that the AgNW network is torn into isolated island structures upon stretching. Thermal transport within these island-like structures happens in an isotropic fashion, which shows that the anisotropic orientation of the TPU fiber network is only partially transferred to the AgNW network and counteracted by the evolution of gaps between such islands parallel to the

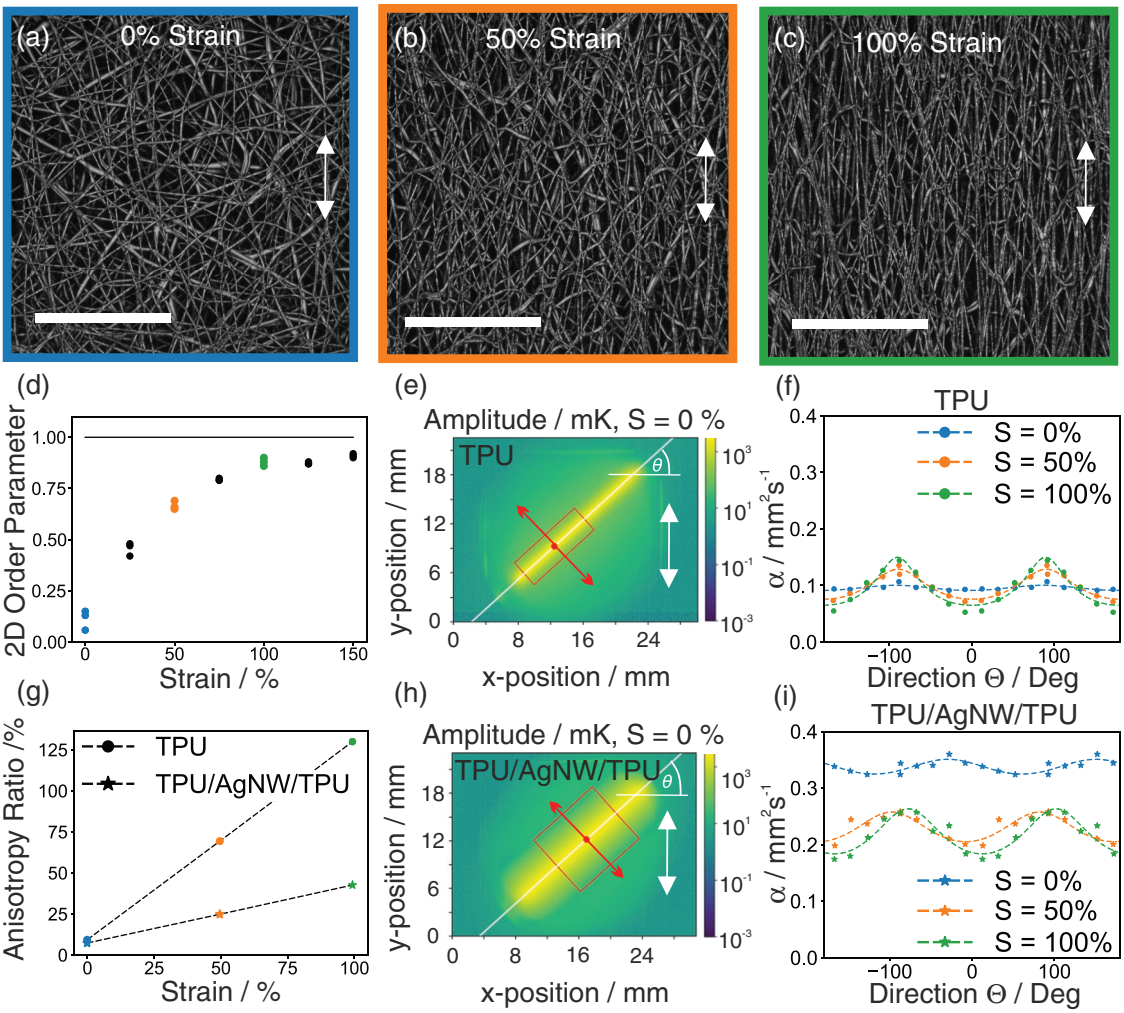

Figure 4. a–c) Laser scanning microscopy images of TPU fibers on the surface of a TPU nonwoven (scale bars: 50 µm). The fibers align in the stretching direction (white arrows) with increasing strain, *S*. d) The 2D order parameter for the fiber orientation, derived from laser scanning microscopy images, increases from 0.1 to 0.9 with increasing strain. e) Temperature amplitude as a function of position on the surface of a pure TPU. f) Thermal diffusivity as a function of direction (0° is horizontal) and strain for a pure TPU (f). The TPU nonwovens are stretched vertically (+/− 90° direction). Anisotropy ratios for the thermal diffusivity. g) The pure TPU shows a stronger anisotropy than the TPU-2.0AgNW/PCL-TPU. h) Temperature amplitude as a function of position on the surface of TPU-2.0AgNW/PCL-TPU film with 0% strain. i) Thermal diffusivity as a function of direction (0° is horizontal) and strain for TPU-2.0AgNW/PCL-TPU film. The films are stretched vertically (+/− 90° direction).

stretching direction. We corroborate this interpretation with additional orientation analysis of AgNW-TPU samples upon stretching, summarized in Figures S12 and S13, Supporting Information.

We now focus on the reversibility of the stretching/compression process and its implications for electromobility measurements. The membranes, even with very high amounts of AgNWs (TPU-2.0AgNW/PCL-TPU), showed excellent stretchability and bending stability. The samples were subjected to 100 cycles of stretching (**Figure 5**a) and bending (Figure 5b). The resistance change can be described by

$$RC = R/R_0 \quad (2)$$

where R is the time dependent resistance and R_0 is the initial resistance. Both R and R_0 were measured after stretching and bending tests to prove the stability after deformation. The RC of TPU-0.25AgNW/PCL-TPU with only 1.2 wt% of AgNWs significantly increased after only 60 stretching cycles, the RC was >20 000 under 50% strain. However, the same sample showed a much better bending stability (bending curvature from 0° to 150°) without a significant change in resistance. The RC of TPU-0.25AgNW/PCL-TPU after 100 bending cycles was merely 1.32. The sample TPU-2.0AgNW/PCL-TPU with a dense network of AgNWs showed both excellent bending and stretching stability. No significant change in the RC was observed for bending tests. During strain testing RC increased by only a factor of ≈20 after 100 cycles. It is important to note that our method of fabrication is particularly suitable to adjust the AgNW concentration in a simple manner. This can even be achieved locally by filtration through a mask. In Figure S14, Supporting Information, we demonstrate, that the local variation of the AgNW concentrations leads to locally confined heating powers. Hence the AgNW

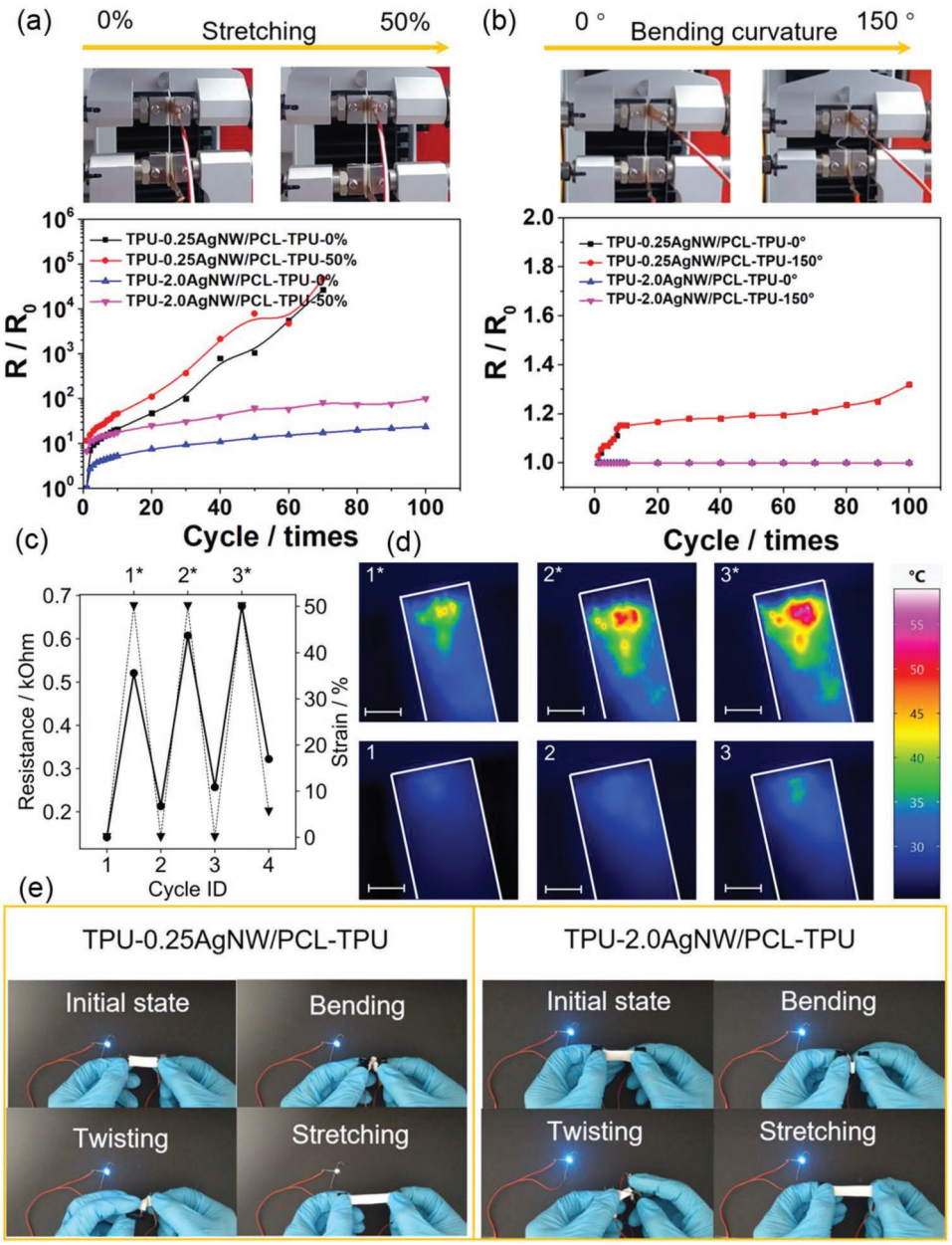

Figure 5. a) Resistance change after 100-cycle stretching test (50% strain). b) Resistance change ratio after 100-cycle bending test (bending curvature from 0° to 150°). Noticing that the bending angle of samples was close to 150° when distance between two clips decreased to 50%. c) Electric resistance (dots) and strain (triangles) during the cycling for the thermographic imaging. d) Thermographic images of a TPU-1.0AgNW/PCL-TPU film during cycling to 50% strain. (scale bars: 5 mm); a constant current of 10 mA passes through the film. The hotspots occur mainly in the stretched state and at different positions from cycle to cycle. e) Digital image of LED brightness by different operation of nonwoven TPU-0.25AgNW/PCL-TPU and TPU-2.0AgNW/PCL-TPU.

concentration, sheet resistance, and response to stretching or bending can be laterally adjusted and optimized for a given application.

We also investigated the changes to the AgNW upon repeated stretching and un-stretching with thermography. This measurement was conducted using a sample of intermediate AgNW concentration (TPU-1.0AgNW/PCL-TPU, 3.5 wt%). Upon stretching (50% strain) we measured an increase in electrical resistance, which translated into hot spot areas. Consistent with our previous analysis such islands of AgNW network (Figure 3d) almost completely disappear upon release of the strain. In the following stretching cycles these hot-spots reform and increase in number and evolved heat. With this intermediate AgNW concentration, a disconnection between the well conducting AgNW islands happens easier and the re-formation of the intact network becomes less complete, in contrast to the better performing samples with a higher amount of AgNWs.

An LED was utilized to demonstrate the flexibility of the prepared sandwich membrane under various mechanical loads during working conditions. TPU-0.25AgNW/PCL-TPU was connected to a circuit, as shown in Figure 5e, and was bent and twisted. The LED maintained almost the same brightness. However, after 50% strain stretching, the brightness of the LED could hardly be observed. This behavior corroborates the formation of a very high RC of TPU-0.25AgNW/PCL-TPU after stretching. When using a more highly concentrated AgNW network (TPU-2.0AgNW/PCL-TPU) twisting, bending, and stretching (50% strain) are tolerated and the brightness of the LED remained almost unchanged. In addition, detailed information is shown in Video S3, Supporting Information.

The use of TPU-2.0AgNW/PCL-TPU as resistive-type strain sensor[31] in a preliminary test for monitoring finger and wrist bending and unbending movements for several times (Figure S15, Supporting Information) worked very well. The sensitivity and precision would be further investigated and other application areas will also be explored.

3. Conclusion

In conclusion, we proposed a new strategy to fabricate sandwich-like electrically conductive membranes with very low electric resistance. Our material consists of an AgNW network sandwiched between two porous electrospun TPU nonwovens. PCL short fibers act as glue and provide a strong interface between the three layers. Our membranes show good bending and stretching stability, high stretchability (breaking elongation more than 700%) and very low initial electric resistance, as low as <0.1 Ω sq^{-1} depending upon the amount of AgNWs. This composite structure shows potential for use as a strain sensor to monitor body movement. Additionally, the membrane possesses gas permeability and low thermal diffusivity. Furthermore, our material has the potential to be integrated into smart wearable devices to collect body movement signals using a connected PC or mobile phone in the future.

4. Experimental Section

Materials: In this study, TPU (Desmopann DP 2590, Bayer Materials Science, M_n 88 900, M_w 145 000), PCL (Capa 6800, M_w 120 000, Perstorp UK Ltd.), poly(vinylpyrrolidone) (PVP K30, M_w 40 000, Sigma-Aldrich), ethylene glycol (p.a. ≥99.5%, Fluka), silver nitrate ($AgNO_3$, p.a. 99.9999%, Sigma-Aldrich), iron chloride ($FeCl_3$, p.a. 98.0%, Sigma-Aldrich), sodium chloride (NaCl, p.a. 99.0%), and dimethylformamide (DMF, p.a. 99.8%) were used as obtained. Other solvents were distilled before use. The AgNWs were synthesized using a previous method.[4]

Analytical Instruments and Methods: A Zeiss LEO 1530 (Jena, Germany; Schottky field-emission cathode) was used for SEM characterization of the AgNWs and their corresponding networks. EDX was performed using a Zeiss Ultra Plus (Jena, Germany; acceleration voltage of 10 kV). TEM measurements were performed using an elastic bright-field transmission electron microscope (TEM, Zeiss 922 Omega EFTEM) at a voltage of 200 kV. ImageJ software was used to determine the AgNW diameter. An average of 100 AgNWs was taken for the diameter calculation.

The AgNW content was determined from thermogravimetric analysis (TGA Libra F1, Netzsch, Selb, Germany). A heating rate of 20 °C min^{-1} was used. The measurements were performed in synthetic air.

Pore size measurements were performed with a PSM 165/H (Dresden, Germany) to determine the pore size. Topor was used as the standard test liquid (surface tension = 16.0 mN m^{-1}). The sample holder had a diameter of 11 mm, and a flow rate of up to 70 L min^{-1} was applied. At least three measurements were carried out for each sample, and an average was taken.

The gas permeability test was performed with a homemade unit as described in our previous work in reference 3. The membrane was fixed at the bottleneck with the cap. A rubber tube (airtight) was used to connect to another glass bottle containing solid carbon dioxide. The glass bottle fixing the nonwovens at the bottleneck was immersed in a phenolphthalein/limewater mixture. The carbon dioxide permeated through the membrane and discolored the aqueous basic solution containing phenolphthalein indicator.

Tensile tests were carried out (sample length 2 cm, width 2 mm) using a tensile tester (ZwickiLine Z0.5; BT1-FR0.5TN. D14; Zwick/Roell, Germany). The following parameters were used: clamping length 1 cm, crosshead speed 10 mm min^{-1}, temperature 20 °C and pretension 0.01 N mm^{-1}. The thickness of the samples was measured with a screw micrometer. The 100-cycle stretching test with 50% and 100% strain was also measured with the abovementioned measuring conditions.

Sheet resistance measurements (four-point measurements) were performed using a Keithley 2420 high-current source meter coupled with a Signatone SYS-301. The sheet resistance was measured ten times for each sample.

A tensile tester (ZwickiLine Z0.5; BT1-FR0.5TN. D14; Zwick/Roell, Germany) was employed to control the stretching distance and bending degree, and a digital multimeter (EMOS Multimeter EM391) connected to measure the sample with a bronze conductor was employed to measure the stretching resistance and bending resistance. The size of the sample and the measuring parameters used here were the same as those used in the tensile test.

Thermography imaging was performed with an Infratec VarioCAM HD research IR camera (7.5–14 µm). The spatial resolution is 29 µm at closest proximity. All measurements were performed in air. The resistance was measured simultaneously with a Keithley 2400 Sourcemeter. The Sourcemeter acted as a constant current source during the four wire resistance measurements. A home built stretching apparatus was used to elongate the samples. The strain was determined from the length change.

Thermal diffusivity was measured with our own, self-built Lock-In thermography setup.[32] Briefly, the films are mounted on a stretchable holder inside a vacuum chamber. An intensity modulated line laser is focused onto the back side of the sample. The intensity modulation creates temperature oscillations inside the thin film. We then detect the surface temperature with a Infratec VarioCAM HD research IR camera. The samples were coated with 25 nm of carbon on both sides to enhance laser absorption and IR emission. The IRBIS active online software from the IR Camera detects amplitude and phase of the temperature fluctuations on the sample surface. The thermal diffusivity is extracted from the material by fitting the linearized amplitude and phase signal, which spreads perpendicular to the line laser excitation.

Optical microscopy was performed on a LEXT Olympus OLS 5000 confocal laser scanning microscope. A 100x magnification lens with a working distance of 300 µm was used. Image analysis was conducted with the Matlab code published by Persson et al.[29]

Preparation of TPU Nonwoven and PCL Short Fibers: Electrospinning of 16 wt% TPU in DMF/THF (80/20 wt%) was carried out to obtain TPU nonwovens with randomly oriented fibers. A round 325 mesh stain-less sieve (70 mm in diameter) at an electrode distance of 15 cm was used as the collector. Other spinning conditions were as follows: positive voltage = 15 kV; temperature = 25 °C; relative humidity = 35%. For spinning PCL, a 15 wt% solution in a mixture of THF/DMF (70/30 wt%) was used. Other electrospinning conditions were the same as those used for TPU spinning. The dispersion (1 g L^{-1}) of short PCL nanofibers was obtained as reported previously by us.[3]

Preparation of Sandwich TPU-AgNW/PCL-TPU Membranes: The preparation procedure for the sandwich membranes is shown

schematically in Figure 1. First, a TPU nonwoven prepared according to the procedure described above via electrospinning was used as a filter. Then, a dispersion of AgNWs and PCL short fibers was filtered. The AgNWs and PCL short fibers formed a conductive layer on top of the TPU nanofiber nonwoven. The fibers were dried under vacuum for 10 min at a pressure of 0.1 mbar. Later, another layer of TPU nanofibers was electrospun on top of the nonwoven with AgNWs and PCL short fibers to construct a flexible, sandwich-like, electrically conductive nonwoven. To induce thermal annealing, the achieved sandwich-like, electrically conductive nonwovens were pressed between two glass plates and heated at a temperature of 75 °C for 30 min to melt the PCL fibers and bond the two layers of TPU nonwovens and AgNWs together.

Supporting Information

Supporting Information is available from the Wiley Online Library or from the author.

Acknowledgements

Qiang Gao would like to thank the China Scholarship Council for awarding a fellowship for carrying out Ph.D. research in Germany in the lab of Prof. Andreas Greiner. Bernd A. F. Kopera acknowledges support from the Elite Network of Bavaria. Financial support by DFG (project GR 972/46-2) and Volkswagen Foundation is acknowledged.

Conflict of Interest

The authors declare no conflict of interest.

Keywords

electrospun membranes, flexible conductors, low resistance, thermal anisotropy

Received: September 12, 2019
Revised: December 3, 2019
Published online: January 9, 2020

[1] a) E. J. Markvicka, M. D. Bartlett, X. N. Huang, C. Majidi, *Nat. Mater.* **2018**, *17*, 618; b) Y. J. Hong, H. Jeong, K. W. Cho, N. Lu, D. H. Kim, *Adv. Funct. Mater.* **2019**, *29*, 1808247; c) S. Y. Huang, Y. Liu, Y. Zhao, Z. F. Ren, C. F. Guo, *Adv. Funct. Mater.* **2019**, *29*, 1805924.

[2] S. H. Jiang, S. Reich, B. Uch, P. Hu, S. Agarwal, A. Greiner, *ACS Appl. Mater. Interfaces* **2017**, *9*, 34286.

[3] Y. Zhou, C. J. Wan, Y. S. Yang, H. Yang, S. C. Wang, Z. D. Dai, K. J. Ji, H. Jiang, X. D. Chen, Y. Long, *Adv. Funct. Mater.* **2019**, *29*, 1806220.

[4] S. Reich, M. Burgard, M. Langner, S. Jiang, X. Wang, S. Agarwal, B. Ding, J. Yu, A. Greiner, *npj Flexible Electron.* **2018**, *2*, 5.

[5] Y. Q. Zeng, T. Li, Y. G. Yao, T. Y. Li, L. B. Hu, A. Marconnet, *Adv. Funct. Mater.* **2019**, *29*, 1901388.

[6] a) W. Weng, P. N. Chen, S. S. He, X. M. Sun, H. S. Peng, *Angew. Chem., Int. Ed.* **2016**, *55*, 6140; b) S. Lee, S. Shin, S. Lee, J. Seo, J. Lee, S. Son, H. J. Cho, H. Algadi, S. Al-Sayari, D. E. Kim, T. Lee, *Adv. Funct. Mater.* **2015**, *25*, 3114; c) J. Lee, B. L. Zambrano, J. Woo, K. Yoon, T. Lee, *Adv. Mater.* **2019**, 1902532.

[7] R. Cao, X. J. Pu, X. Y. Du, W. Yang, J. N. Wang, H. Y. Guo, S. Y. Zhao, Z. Q. Yuan, C. Zhang, C. J. Li, Z. L. Wang, *ACS Nano* **2018**, *12*, 5190.

[8] M. Amjadi, M. Sitti, *Adv. Sci.* **2018**, *5*, 1800239.

[9] R. P. Tong, G. X. Chen, D. H. Pan, H. S. Qi, R. A. Li, J. F. Tian, F. C. Lu, M. H. He, *Biomacromolecules* **2019**, *20*, 2096.

[10] a) A. Chortos, J. Liu, Z. Bao, *Nat. Mater.* **2016**, *15*, 937; b) S. H. Wang, J. Y. Oh, J. Xu, H. Tran, Z. Bao, *Acc. Chem. Res.* **2018**, *51*, 1033; c) Y. Lee, J. Park, A. Choe, S. Cho, J. Kim, H. Ko, *Adv. Funct. Mater.* **2019**, 1904523.

[11] C. Majidi, *Adv. Mater. Technol.* **2019**, *4*, 1800477.

[12] G. Chen, N. Matsuhisa, Z. Y. Liu, D. P. Qi, P. Q. Cai, Y. Jiang, C. J. Wan, Y. J. Cui, W. R. Leow, Z. J. Liu, S. X. Gong, K. Q. Zhang, Y. Cheng, X. D. Chen, *Adv. Mater.* **2018**, *30*, 1800129.

[13] a) T. H. Kim, C. S. Lee, S. Kim, J. Hur, S. Lee, K. W. Shin, Y. Z. Yoon, M. K. Choi, J. Yang, D. H. Kim, T. Hyeon, S. Park, S. Hwang, *ACS Nano* **2017**, *11*, 5992; b) H. S. Liu, B. C. Pan, G. S. Liou, *Nanoscale* **2017**, *9*, 2633.

[14] A. D. Valentine, T. A. Busbee, J. W. Boley, J. R. Raney, A. Chortos, A. Kotikian, J. D. Berrigan, M. F. Durstock, J. A. Lewis, *Adv. Mater.* **2017**, *29*, 1703817.

[15] H. H. Shi, N. Khalili, T. Morrison, H. E. Naguib, *ACS Appl. Mater. Interfaces* **2018**, *10*, 19037.

[16] a) N. Karim, S. Afroj, S. R. Tan, P. He, A. Fernando, C. Carr, K. S. Novoselov, *ACS Nano* **2017**, *11*, 12266; b) C. Zhu, A. Chortos, Y. Wang, R. Pfattner, T. Lei, A. C. Hinckley, I. Pochorovski, X. Yan, J. W. F. To, J. Y. Oh, J. B. H. Tok, Z. Bao, B. Murmann, *Nat. Electron.* **2018**, *1*, 183.

[17] M. Tavakoli, M. H. Malakooti, H. Paisana, Y. Ohm, D. G. Marques, P. A. Lopes, A. P. Piedade, A. T. de Almeida, C. Majidi, *Adv. Mater.* **2018**, *30*, 1801852.

[18] H. Lee, M. Kim, I. Kim, H. Lee, *Adv. Mater.* **2016**, *28*, 4541.

[19] P. C. Hsu, X. Liu, C. Liu, X. Xie, H. R. Lee, A. J. Welch, T. Zhao, Y. Cui, *Nano Lett.* **2015**, *15*, 365.

[20] S. J. Benight, C. Wang, J. B. H. Tok, Z. Bao, *Prog. Polym. Sci.* **2013**, *38*, 1961.

[21] K. Arapov, E. Rubingh, R. Abbel, J. Laven, G. de With, H. Friedrich, *Adv. Funct. Mater.* **2016**, *26*, 586.

[22] S. Kustra, H. Wu, S. Basu, G. K. Rohde, C. J. Bettinger, *Small* **2012**, *8*, 3746.

[23] B. R. Yang, W. Cao, G. S. Liu, H. J. Chen, Y. Y. Noh, T. Minari, H. C. Hsiao, C. Y. Lee, H. P. Shieh, C. Liu, *ACS Appl. Mater. Interfaces* **2015**, *7*, 21433.

[24] J. W. Yoon, W. S. Chang, S. H. Cho, *Opt. Lasers Eng.* **2015**, *73*, 40.

[25] F. Xu, Y. Zhu, *Adv. Mater.* **2012**, *24*, 5117.

[26] V. Martinez, F. Stauffer, M. O. Adagunodo, C. Forro, J. Voros, A. Larmagnac, *ACS Appl. Mater. Interfaces* **2015**, *7*, 13467.

[27] Y. J. Fan, X. Li, S. Y. Kuang, Y. Kuang, L. Zhang, Y. H. Chen, L. Liu, K. Zhang, S. W. Ma, F. Liang, T. Wu, Z. L. Wang, G. Zhu, *ACS Nano* **2018**, *12*, 9326.

[28] Z. Jiang, M. O. G. Nayeem, K. Fukuda, S. Ding, H. Jin, T. Yokota, D. Inoue, D. Hashizume, T. Someya, *Adv. Mater.* **2019**, *31*, 1903446.

[29] N. E. Persson, M. A. McBride, M. A. Grover, E. Reichmanis, *Chem. Mater.* **2017**, *29*, 3.

[30] J. Liu, R. Yang, *Phys. Rev. B* **2010**, *81*, 174122.

[31] a) J.-H. Kim, S.-R. Kim, H.-J. Kil, Y.-C. Kim, J.-W. Park, *Nano Lett.* **2018**, *18*, 4531; b) S. Chen, S. Zeng, S. Liu, H. Liu, R. Zheng, K. L. White, A. T. Smith, L. Liu, L. Sun, *Chem. Mater.* **2019**, *31*, 8708.

[32] a) A. Philipp, N. W. Pech-May, B. A. F. Kopera, A. M. Lechner, S. Rosenfeldt, M. Retsch, *Anal. Chem.* **2019**, *91*, 8476; b) H. M. Akram, M. Maqsood, H. Rashid, *Rev. Sci. Instrum.* **2009**, *80*, 075103.